

The advection-dominated accretion flow for the origin of the thermal soft X-ray component in low-level accreting neutron stars

Erlin Qiao ^{1,2}^{*} and B.F. Liu ^{1,2}

¹Key Laboratory of Space Astronomy and Technology, National Astronomical Observatories, Chinese Academy of Sciences, Beijing 100012, China

²School of Astronomy and Space Sciences, University of Chinese Academy of Sciences, 19A Yuquan Road, Beijing 100049, China

Accepted XXX. Received YYY; in original form ZZZ

ABSTRACT

A thermal soft X-ray component is often detected in low-level accreting neutron stars (NSs), but is not detected in low-level accreting stellar-mass black holes (BHs). In this paper, we investigate the origin of such a thermal soft X-ray component in the framework of the self-similar solution of the advection-dominated accretion flow (ADAF) around NSs. It is assumed that a fraction, f_{th} , of the energy transferred onto the surface of the NS is thermalized at the surface of the NS as the soft photons to be scattered in the ADAF. We self-consistently calculate the structure and the corresponding emergent spectrum of the ADAF by considering the radiative coupling between the soft photons from the surface of the NS and the ADAF itself. We show that the Compton y -parameter of the ADAF for NSs is systematically lower than that of BHs. Meanwhile, we find that the temperature of the thermal soft X-ray component in NSs decreases with decreasing mass accretion rate, which is qualitatively consistent with observations. We test the effect of f_{th} on the structure, as well as the emergent spectrum of the ADAF. It is found that a change of f_{th} can significantly change the temperature of the thermal soft X-ray component as well as the spectral slope in hard X-rays. Finally, it is suggested that the value of f_{th} can be constrained by fitting the high-quality X-ray data, such as the *XMM-Newton* spectrum between 0.5–10 keV in the future work.

Key words: accretion, accretion discs – stars; neutron – black hole physics – X-rays; binaries

1 INTRODUCTION

Low-mass X-ray binaries (XRBs) are accreting systems with either a stellar-mass black hole (BH) or a neutron star (NS) drawing gas from its low-mass companion star ($\lesssim 1M_{\odot}$) via its Roche lobe. Most of the low-mass XRBs are X-ray transients, which are discovered when they first go into outburst. The outburst can last from a few weeks to a few months, then decayed into quiescence for months to years (Tanaka & Lewin 1995; Remillard & McClintock 2006). Generally, there are two dominated spectral states in both BHXRBs and NSXRBs, i.e., the high/soft spectral state with a relatively higher mass accretion rate, and the low/hard spectral state with a relatively lower mass accretion rate (Done et al. 2007; Gilfanov 2010). The soft-to-hard state transition occurs at about 1 – 4% of the Eddington luminosity (Maccarone 2003), while for some sources, the hysteresis is observed, i.e., the transition luminosity of the soft-to-hard state transition is ~ 3 times lower than of the transition luminosity of the hard-to-soft transition (e.g. Maccarone & Coppi 2003; Nowak et al. 2002; Kubota & Done 2004; Rodriguez et al. 2003; Meyer-Hofmeister et al. 2005; Gladstone et al. 2007; Zhang et al.

2016; Zhang & Yu 2018). So far, a great of effects have been made for exploring the accretion physics in the different spectral states of XRBs. Currently, it is widely believed that in the high/soft state, the accretion is dominated by the cool, geometrically thin, optically thick disc (Shakura & Sunyaev 1973). While in the low/hard spectral state, the accretion is dominated by the hot, optically thin, advection-dominated accretion flow (ADAF) (Narayan & Yi 1994, 1995; Yuan & Narayan 2014, for review).

Theoretically, for the ADAF around astrophysical BHs, a fraction of the viscously dissipated energy in the ADAF will be advected into the event horizon of the BHs rather than being radiated out (Ichimaru 1977; Rees et al. 1982; Narayan & Yi 1994; Abramowicz et al. 1995; Chen et al. 1995). The fraction of the energy advected into the black hole depends on the mass accretion rate. Specifically, for a relatively higher mass accretion rate within the ADAF regime, such as the mass accretion rate close to the rate corresponding to the spectral state transition in BHXRBs, the fraction of the energy advected into the black hole is small, and the radiative efficiency of the ADAF can be nearly comparable with that of the cool disc (Xie & Yuan 2012). The radiative efficiency of the ADAF decreases rapidly with decreasing mass accretion rate \dot{M} . Especially, if $\dot{M} \lesssim 5 \times 10^{-4} \dot{M}_{\text{Edd}}$ (with $\dot{M}_{\text{Edd}} = 1.39 \times 10^{18} M/M_{\odot} \text{ g s}^{-1}$), the accretion is completely dominated

* E-mail: qiaoe1@nao.cas.cn

by the advection, and the accretion flow is radiatively inefficient (Mahadevan 1997). While for the ADAF around NSs, due to the existence of a hard surface of NSs, it is expected that the energy advected onto the surface of the NSs will eventually be radiated out, so the accretion flow is always radiatively efficient. The observational data indeed support that the quiescent BH accreting systems are fainter than that of the quiescent NS accreting systems with similar mass accretion rates, as can be seen in the diagram between the luminosity and the binary orbital period (e.g. Menou et al. 1999; Lasota 2000; Garcia et al. 2001; Hameury et al. 2003; McClintock et al. 2004). The study of Narayan & Yi (1995) showed that there exists a critical mass accretion rate \dot{M}_{crit} . For $\dot{M} \gtrsim \dot{M}_{\text{crit}}$, the accretion flow will transit from the hot ADAF to the cool disc. For NS accreting systems, the energy advected onto the surface of the NS will eventually radiate out, which in turn can effectively cool the accretion flow, resulting in the accretion flow much easier to collapse. So theoretically the critical mass accretion rate \dot{M}_{crit} for NSs is generally lower than that of BHs. Specifically, the critical mass accretion rate is $\dot{M}_{\text{crit}} \sim \alpha^2 \dot{M}_{\text{Edd}}$ (with α being the viscosity parameter) for a BH accreting system, while the critical mass accretion rate is $\dot{M}_{\text{crit}} \sim 0.1\alpha^2 \dot{M}_{\text{Edd}}$ for a NS accreting system (Narayan & Yi 1995).

Observationally, in low-level accreting NSs with the 0.5 – 10 keV X-ray luminosity in the range of about 10^{34} to 10^{36} erg s^{-1} corresponding to 0.01% – 1% of the Eddington luminosity, a thermal soft X-ray component is detected (e.g. Jonker et al. 2004; Armas Padilla et al. 2013a,b; Degenaar et al. 2013a; Campana et al. 2014). While such a thermal soft X-ray component is not detected in accreting BHs in the similar luminosity range (e.g. Wijnands et al. 2015). In some low-level accreting NSs, it is found that the temperature of such a thermal soft X-ray component decreases with decreasing the X-ray luminosity, which implies that the origin of such a thermal soft X-ray component in low-level accreting NSs is accretion-related (Armas Padilla et al. 2013c; Degenaar et al. 2013a; Bahramian et al. 2014). By fitting the X-ray spectrum of a sample composed of twelve BH and NS XRBs, it is found that the electron temperature T_e of the corona around NSs is $\sim 15 - 25$ keV, while the electron temperature T_e is $\sim 30 - 200$ keV around BHs. Meanwhile, it is found that the Compton y -parameter for NSs is systemically lower than that of BHs (Burke et al. 2017). The lower electron temperature and the lower Compton y -parameter of the corona for NSs compared with the case for BHs are believed to be resulted by the strong Compton cooling of the corona by the soft thermal photons from the surface of the NSs (Sunyaev & Titarchuk 1989; Syunyaev et al. 1991; Narayan & McClintock 2008).

The very faint X-ray binary IGR J17062-6143 discovered in 2006 is believed to be a NSXRB due to the detection of a Type-I X-ray burst in 2012 (Degenaar et al. 2013b). By fitting the spectral energy distribution (SED) of IGR J17062-6143, it was shown that the thermal soft X-ray component can not originate from the accretion disc (Hernandez Santisteban et al. 2018). van den Eijnden et al. (2018) fitted the soft X-ray data of IGR J17062-6143 in three different epochs, i.e., 2014 (*Chandra*), 2015 (*Swift*), and 2016 (*XMM-Newton*), suggesting that the thermal soft X-ray component is from the surface of the NS with a radius $\sim 11 - 12$ km. Furthermore, it is found that the temperature of the thermal soft X-ray component decreases from 0.48 ± 0.01 keV (2014) and 0.47 ± 0.01 keV (2015) in the first two epochs to 0.36 ± 0.01 keV (2016) with ~ 2 times decrease of the X-ray luminosity (van den Eijnden et al. 2018), which are qualitatively con-

sistent with the theoretical predictions of the low-level accretion around NSs (Zampieri et al. 1995).

In this paper, we investigate the origin of such a thermal soft X-ray component in low-level accreting NSs based on the self-similar solution of the ADAF (Narayan & Yi 1995). Specifically, we consider that the internal energy stored in the ADAF and the radial kinetic energy of the ADAF are transferred onto the surface of the NS. A fraction, f_{th} , of this energy is assumed to be thermalized as the blackbody emission, which is then scattered in the ADAF. We self-consistently calculate the structure of the ADAF by considering the coupling of the blackbody emission from the surface of the NS and the ADAF itself. With the derived structure of the ADAF, we adopt the multi-scattering method to calculate the emergent of the ADAF around NSs. We compare the structure and the emergent spectrum of the ADAF between BHs and NSs. We study the structural and the spectral features of the ADAF with the mass accretion rates, especially, the temperature of the thermal soft X-ray component with the mass accretion rates. We test the effect of f_{th} on the structural and the spectral features of the ADAF with a focus on the relationship between the temperature of the thermal soft X-ray component and f_{th} . The model is briefly introduced in Section 2. The numerical results are shown in Section 3. The discussions are in Section 4, and the conclusions are in Section 5.

2 THE MODEL

In this paper, we calculate the structure of the ADAF around a NS or a BH based on the self-similar solution of the ADAF (Narayan & Yi 1995). For clarity, we list the equations as follows.

Equation of state,

$$p_g = \beta \rho c_s^2 = \frac{\rho k T_i}{\mu_i m_p} + \frac{\rho k T_e}{\mu_e m_p}, \quad (1)$$

where p_g is the gas pressure, m_p is the proton mass, and β is the magnetic parameter (with magnetic pressure $p_m = B^2/8\pi = (1 - \beta)p$, $p = p_g + p_m$), T_i is the ion temperature and T_e is the electron temperature, ρ is the density, k is the Boltzmann constant, μ_i and μ_e are the effective molecular weights of ions and electrons respectively, which can be expressed as,

$$\mu_i = \frac{4}{1 + 3X} = 1.23, \quad \mu_e = \frac{2}{1 + X} = 1.14, \quad (2)$$

where the hydrogen mass fraction $X = 0.75$ is adopted for the numerical values of μ_i and μ_e . The internal energy per unit volume of the gas is,

$$U = \frac{3}{2} p_g + \frac{B^2}{4\pi}. \quad (3)$$

In the following, we list the radial velocity v , the angular velocity Ω , the isothermal sound speed c_s , the density ρ , the magnetic field B , the pressure p , the electron number density n_e , the viscous dissipation of energy per unit volume q^+ , and the scattering optical depth τ_{es} in the vertical direction derived from the self-similar solution of the ADAF, which are all functions of m , \dot{m} , α , β and r

(Narayan & Yi 1995),

$$\begin{aligned}
 v &= -2.12 \times 10^{10} \alpha c_1 r^{-1/2} \text{ cm s}^{-1}, \\
 \Omega &= 7.19 \times 10^4 c_2 m^{-1} r^{-3/2} \text{ s}^{-1}, \\
 c_s^2 &= 4.50 \times 10^{20} c_3 r^{-1} \text{ cm}^2 \text{ s}^{-2}, \\
 \rho &= 3.79 \times 10^{-5} \alpha^{-1} c_1^{-1} c_3^{-1/2} m^{-1} \dot{m} r^{-3/2} \text{ g cm}^{-3}, \\
 p &= 1.71 \times 10^{16} \alpha^{-1} c_1^{-1} c_3^{1/2} m^{-1} \dot{m} r^{-5/2} \text{ g cm}^{-1} \text{ s}^{-2}, \\
 B &= 6.55 \times 10^8 \alpha^{-1/2} (1-\beta)^{1/2} c_1^{1/2} c_3^{1/4} m^{-1/2} \dot{m}^{1/2} r^{-5/4} \text{ G}, \\
 n_e &= \rho / \mu_e m_p = 2.00 \times 10^{19} \alpha^{-1} c_1^{-1} c_3^{-1/2} m^{-1} \dot{m} r^{-3/2} \text{ cm}^{-3}, \\
 q^+ &= 1.84 \times 10^{21} \varepsilon' c_3^{1/2} m^{-2} \dot{m} r^{-4} \text{ ergs cm}^{-3} \text{ s}^{-1}, \\
 \tau_{\text{es}} &= 2n_e \sigma_T H = 12.4 \alpha^{-1} c_1^{-1} \dot{m} r^{-1/2},
 \end{aligned} \tag{4}$$

where m is the mass of a NS or a BH scaled with the solar mass M_\odot , \dot{m} is the accretion rate scaled with the Eddington accretion rate \dot{M}_{Edd} , r is the radius from the black hole scaled with the Schwarzschild radius R_S (with $R_S = 2.95 \times 10^5 m \text{ cm}$), and

$$\begin{aligned}
 c_1 &= \frac{(5+2\varepsilon')}{3\alpha^2} g(\alpha, \varepsilon'), \\
 c_3 &= \frac{2\varepsilon(5+2\varepsilon')}{9\alpha^2} g(\alpha, \varepsilon'), \\
 \varepsilon' &= \frac{\varepsilon}{f} = \frac{1}{f} \left(\frac{5/3-\gamma}{\gamma-1} \right),
 \end{aligned} \tag{5}$$

$$\begin{aligned}
 g(\alpha, \varepsilon') &= \left[1 + \frac{18\alpha^2}{(5+2\varepsilon')^2} \right]^{1/2} - 1, \\
 \gamma &= \frac{32-24\beta-3\beta^2}{24-21\beta},
 \end{aligned}$$

with f being the advected fraction of the viscously dissipated energy. The energy balance of the ADAF is determined by the following equations,

$$\begin{aligned}
 q^+ &= f q^+ + q^{\text{ie}} \\
 q^{\text{ie}} &= q^-
 \end{aligned} \tag{6}$$

where q^{ie} is the energy transfer rate from ions to electrons via Coulomb collision (Stepney 1983), which is given by,

$$q_{\text{ie}} = 3.59 \times 10^{-32} n_e n_i (T_i - T_e) \frac{1+T'^{1/2}}{T'^{3/2}}, \tag{7}$$

with

$$T' = \frac{kT_e}{m_e c^2} \left(1 + \frac{m_e}{m_p} \frac{T_i}{T_e} \right), \tag{8}$$

and m_e is the electron mass, c is the speed of light. $q^- = q_{\text{brem}}^- + q_{\text{syn}}^- + q_{\text{brem,C}}^- + q_{\text{syn,C}}^- + q_{*C}^-$ is the cooling rate of the electrons with q_{brem}^- , q_{syn}^- , $q_{\text{brem,C}}^-$, $q_{\text{syn,C}}^-$ and q_{*C}^- being the bremsstrahlung cooling rate, the synchrotron cooling rate, the Compton cooling rate by self-Comptonization of bremsstrahlung radiation, the Compton cooling rate by self-Comptonization of synchrotron radiation, and the Compton cooling rate by Comptonization of the radiation from the central NS. The expressions for q_{brem}^- , q_{syn}^- , $q_{\text{brem,C}}^-$, $q_{\text{syn,C}}^-$ are all the standard expressions as in (Narayan & Yi 1995).

Here for NSs, we consider that the dominated soft photons from the surface of the NS to be scattered in the accretion flow are from the accretion itself. Specifically, we consider that the internal energy and the radial kinetic energy of the ADAF was transferred onto the surface of the NS. A fraction f_{th} of this energy is assumed to be thermalized as the blackbody emission, which is then scattered in the ADAF. The energy of the ADAF transferred onto the surface of the NS per second can be expressed as,

$$L_* = 4\pi R_* H(R_*) |v(R_*)| \left[U(R_*) + \frac{1}{2} \rho(R_*) v^2(R_*) \right], \tag{9}$$

where R_* is the radius of the NS, and $U(R_*)$ is the internal energy of the gas at R_* as equation (3), $H(R_*)$ is the scaleheight of the gas at R_* , $\rho(R_*)$ and $v(R_*)$ are the density of the gas and the radial velocity of the gas at R_* respectively as in equation (4). In this case, if the radiation from the surface of the NS is assumed to be isotropic, the effective temperature of the radiation T_* can be given by,

$$T_* = \left(\frac{L_* f_{\text{th}}}{4\pi R_*^2 \sigma} \right)^{1/4}, \tag{10}$$

where σ is the Stefan-Boltzmann constant. The outgoing flux from the NS reaching at a radius R is given by,

$$F_*(R) = \left(\frac{L_*}{4\pi R^2} \right) e^{-\tau'_{\text{es}}(R)}, \tag{11}$$

where $\tau'_{\text{es}}(R)$ is the scattering optical depth in the radial direction from the surface of the NS. Such a flux $F_*(R)$ at a distance R is locally scattered in the ADAF, and the Compton cooling rate q_{*C}^- is then derived accordingly. One can refer to equation (3.28-3.30) in (Narayan & Yi 1995) for details. q_{*C}^- is assumed to be zero for BHs due to the existence of the event horizon.

Substituting the formulae of ρ and c_s^2 in equation (4) into equation (1), the equation of state of the gas can be re-expressed as,

$$T_i + 1.08 T_e = 6.66 \times 10^{12} \beta c_3 r^{-1}. \tag{12}$$

We solve equations (6) and (12) for the ion temperature T_i , electron temperature T_e and the advected fraction of the viscously dissipated energy f by specifying the black hole mass m , accretion rate \dot{m} , viscosity parameter α , magnetic parameter β and f_{th} describing the fraction of the internal energy and the radial kinetic energy transferred onto the surface of the NS to be thermalized as the blackbody emission. With the derived electron temperature T_e and the scattering optical depth τ_{es} in the vertical direction, we calculate the corresponding emergent spectrum of the ADAF around a NS with the multi-scattering of photons in the hot gas. One can refer to Qiao & Liu (2010, 2013) or Manmoto et al. (1997) for the calculation of the emergent spectrum for details.

3 NUMERICAL RESULTS

We calculate the structure of the ADAF by specifying m , α , β and f_{th} . Throughout the paper, we take $m = 10$ and $m = 1.4$ for BH and NS respectively. Meanwhile, we take the inner boundary of the ADAF as $3R_S$ for BHs (non-rotating) and 12.5 km^1 for NSs. we set $\alpha = 0.3$ as usual. The magnetic field in the ADAF solution is relatively weak, as suggested by magnetohydrodynamic simulations (Yuan & Narayan 2014). We fix $\beta = 0.95$ in this paper.

3.1 Black hole vs. Neutron star

In the panel (1) of Fig. (1), we plot the ion temperature T_i and the electron temperature T_e of the ADAF as a function of radius for BHs and NSs respectively with $\dot{m} = 5 \times 10^{-3}$. $f_{\text{th}} = 1$ is adopted for NSs. The black-solid line and the black-dashed line are the ion temperature and the electron temperature of the ADAF for BHs respectively. The red-solid line and the red-dashed line are the ion

¹ Assuming the central star with the mass M and radius R_* , the gravitational potential energy released by the accretion of a unit mass to its surface is $\Delta E = GM/R_*$. For a non-rotating black hole, R_* is assumed to be as $3R_S$, so $\Delta E = c^2/6$. In this paper, in order to keep the same energy release by the accretion of a unit mass between the BH and NS, if $m = 1.4M_\odot$ is adopted for a NS, the corresponding radius of a NS is $R_* = 12.5 \text{ km}$.

temperature and the electron temperature of the ADAF for NSs respectively. It is clear that the ion temperature of BHs and NSs is very similar, which intrinsically can be predicted by the basic assumptions set in the ADAF, i.e., the ions are first heated by the viscous process, and then a fraction of this heat energy stored in the ions is transferred to the electrons via Coulomb collision. Since the density of the gas in the ADAF is low, the Coulomb collision is not efficient, the fraction of the heat energy transferred to the electrons is small. Consequently, the ions can keep a relatively higher temperature, which is close to the virial temperature. We note that the electron temperature of BHs is ~ 3 times higher than that of NSs. This can be understood as the strong Compton cooling of the electrons in the ADAF by the soft photons from the surface of the NSs, which however does not exist for BHs. In the panel (2) of Fig. (1), we plot the Compton scattering optical depth τ_{es} as a function of radius for BHs and NSs respectively with $\dot{m} = 5 \times 10^{-3}$. $f_{\text{th}} = 1$ is adopted for NSs. The black line is for BHs and the red line is for NSs. It is shown that the Compton scattering optical depth for BHs is slightly less than that of NSs. In the panel (3) of Fig. (1), we plot the Compton y -parameter (defined as $y = \frac{4kT_e}{m_e c^2} \text{Max}(\tau_{\text{es}}, \tau_{\text{es}}^2)$) as a function of radius for BHs and NSs respectively with $\dot{m} = 5 \times 10^{-3}$. $f_{\text{th}} = 1$ is adopted for NSs. The black line is for BHs and the red line is for NSs. It is found that the Compton y -parameter for BHs is significantly larger than that of NSs, which intrinsically can predict a harder hard X-ray spectrum for BHs compared with NSs. In the panel (4) of Fig. (1), we plot the ratio of the angular velocity of the ADAF to the Keplerian angular velocity, Ω/Ω_{K} (with Ω_{K} being the Keplerian angular velocity), as a function of radius for BHs and NSs respectively with $\dot{m} = 5 \times 10^{-3}$. $f_{\text{th}} = 1$ is adopted for NSs. The black line is for BHs and the red line is for NSs. It can be seen that Ω/Ω_{K} for BHs is systematically lower than that of NSs. As discussed in (Narayan & Yi 1994) for the self-similar solution of the ADAF, $\Omega \approx [2\epsilon'/(5 + 2\epsilon')]^{1/2} \Omega_{\text{K}}$ (with $\epsilon' \propto 1/f$). For the case of very efficient cooling, $f \rightarrow 0$, $\epsilon' \rightarrow \infty$, and $\Omega \rightarrow \Omega_{\text{K}}$. Meanwhile, it is clear that Ω decreases with increasing f . The radiative efficiency of the ADAF around BHs is intrinsically lower than that of NSs, resulting in a lower value of Ω/Ω_{K} for BHs compared with the case for NSs. It is also found that Ω/Ω_{K} increases with increasing radius for NSs, indicating that the angular velocity of the ADAF is closer to the Keplerian value in the outer region. One can refer to Fig. (2) for the corresponding emergent spectra, as the black line is for BHs and the red line is for NSs. In Table (1), we list the related radiative features of the ADAF around BHs and NSs respectively. As an example, for a NS with $\dot{m} = 5 \times 10^{-3}$ and $f_{\text{th}} = 1$, the temperature of the thermal soft X-ray component from the surface of the NS is 0.45 keV, and the X-ray luminosity between 0.5 to 10 keV is 1.0×10^{36} erg s $^{-1}$. While for a BH with $\dot{m} = 5 \times 10^{-3}$, due to the existence of the event horizon, all the internal energy stored in the ADAF and radial kinetic energy of the ADAF at R_* are advected into the event horizon without radiation. So no such a thermal component is predicted for BHs, as can be seen from the emergent spectrum in Fig. (2). The X-ray luminosity between 0.5 to 10 keV for BHs is 2.2×10^{34} erg s $^{-1}$ nearly two orders of magnitude lower than that of NSs, which is also one of the basic conclusions predicted by the ADAF solution, i.e., most of the viscously dissipated energy is advected into the event horizon of the BH without radiation, while the energy advected onto the surface of the NS will be eventually radiated out.

3.2 The dependence of the structure and emergent spectra on \dot{m}

In the panel (1) of Fig. 3, we plot the ion temperature T_i and the electron temperature T_e of the ADAF as a function of radius for NSs for different \dot{m} with $f_{\text{th}} = 1$. It can be seen that both T_i and T_e change very slightly with \dot{m} around NSs, which is very similar to the case of BHs (Mahadevan 1997). In the panel (2) of Fig. (3), we plot the Compton scattering optical depth τ_{es} as a function of radius for NSs for different \dot{m} with $f_{\text{th}} = 1$. The Compton scattering optical depth τ_{es} systemically decreases with decreasing \dot{m} , as predicted by the formula of τ_{es} in equation (4). In the panel (3) of Fig. (3), we plot the Compton y -parameter as a function of radius for NSs for different \dot{m} with $f_{\text{th}} = 1$. It is clear that the Compton y -parameter decreases with decreasing \dot{m} , which predicts a softer hard X-ray spectrum with decreasing \dot{m} , as can be seen in Fig. (4). In the panel (4) of Fig. (3), we plot Ω/Ω_{K} as a function of radius for NSs for different \dot{m} with $f_{\text{th}} = 1$. It can be seen that Ω/Ω_{K} systemically decreases with decreasing \dot{m} , which can be roughly understood as, with a decrease of \dot{m} , the radiative efficiency of the ADAF slightly decreases even in the case of NSs, resulting in a decrease of the angular velocity, as has been discussed in Section 3.1. In Table (2), we list the radiative features of the ADAF around NSs for different \dot{m} with $f_{\text{th}} = 1$. It can be seen that the ratio of the energy of the ADAF transferred onto the surface of the NS per second, L_* , to the accretion luminosity, L_G , (defined as $L_G = GMM/R_*$) slightly increases with decreasing \dot{m} , which however does not affect the trend that the temperature of the thermal soft X-ray component decreases from 0.45 keV to 0.26 keV for the mass accretion rate decreasing from $\dot{m} = 5 \times 10^{-3}$ to $\dot{m} = 5 \times 10^{-4}$. Meanwhile, the X-ray luminosity between 0.5 to 10 keV decreases from 1.0×10^{36} erg s $^{-1}$ to 1.3×10^{35} erg s $^{-1}$ for the mass accretion rate decreasing from $\dot{m} = 5 \times 10^{-3}$ to $\dot{m} = 5 \times 10^{-4}$. It is interesting to note that, a linear correlation between $\log L_{0.5-10\text{keV}}$ and $\log \dot{m}$ is found, i.e.,

$$\log L_{0.5-10\text{keV}} = 38.1 + 0.9 \times \log \dot{m}, \quad (13)$$

which can be simply expressed as $L_{0.5-10\text{keV}} \propto \dot{m}^{0.9}$. The fitting result of $L_{0.5-10\text{keV}} \propto \dot{m}^{0.9}$ for the ADAF around NSs is very close to the predictions by the radiative efficient accretion flows as generally, $L \propto \dot{m}$. For the ADAF around BHs, theoretically, ADAF is radiatively inefficient and $L \propto \dot{m}^s$, with $s \sim 2$ for $5 \times 10^{-3} \lesssim \dot{m} \lesssim 2 \times 10^{-2}$, with $s \sim 1.6$ for $10^{-4} \lesssim \dot{m} \lesssim 5 \times 10^{-3}$, and with $s \sim 3.4$ for $\dot{m} \lesssim 10^{-4}$ (Merloni et al. 2003).

3.3 The effect of f_{th}

In the panel (1) of Fig. (5), we plot the ion temperature T_i and the electron temperature T_e of the ADAF as a function of radius for different f_{th} with $\dot{m} = 5 \times 10^{-3}$. As we can see, T_i nearly does not change with changing f_{th} . While T_e increases with decreasing f_{th} , which can be easily understood as follows. A smaller value of f_{th} means that less energy of the internal energy stored in the ADAF and the radial kinetic energy of the ADAF transferred onto the surface of the NS can be thermalized as the soft photons to cool the accretion flow, consequently predicting a relatively higher T_e . In the panel (2) of Fig. (5), we plot the Compton scattering optical depth τ_{es} as a function of radius for NSs for different f_{th} with $\dot{m} = 5 \times 10^{-3}$. It is shown that there is a slight decrease of τ_{es} with decreasing f_{th} . In the panel (3) of Fig. (5), we plot the Compton y -parameter as a function of radius for NSs for different f_{th} with $\dot{m} = 5 \times 10^{-3}$. It is shown that the Compton y -parameter increases with decreasing f_{th} , which predicts a harder hard X-ray spectrum with

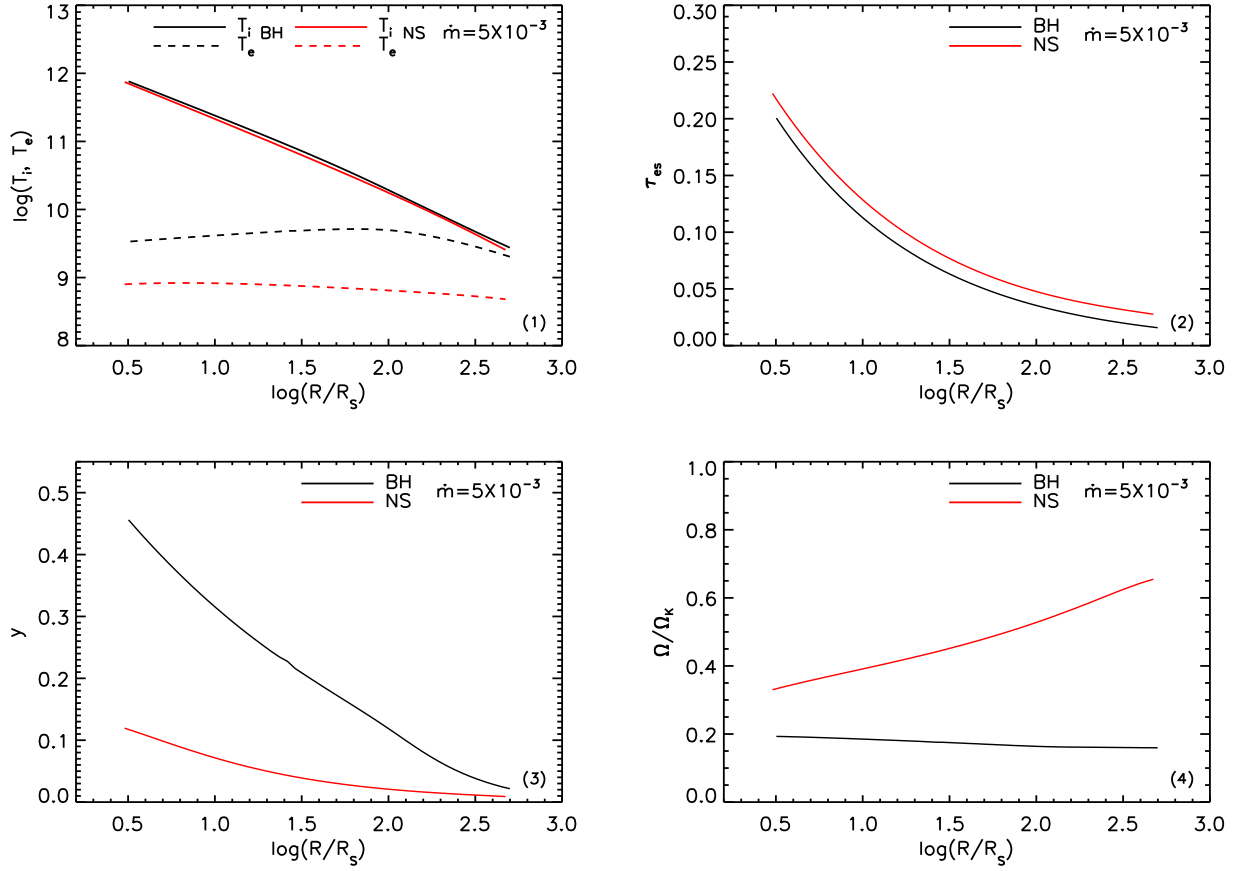


Figure 1. Panel (1): ion temperature T_i (solid line) as a function of radius and electron temperature T_e (dashed line) as a function of radius. The black lines are for BHs and the red lines are for NSs. Panel (2): Compton scattering optical depth τ_{es} as a function of radius. The black line is for BHs and the red line is for NSs. Panel (3): Compton y-parameter as a function of radius. The black line is for BHs and the red line is for NSs. Panel (4): Ω/Ω_K as a function of radius. The black line is for BHs and the red line is for NSs.

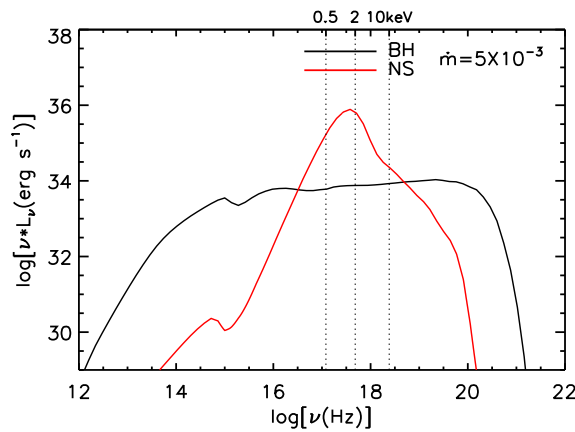


Figure 2. Emergent spectra of the ADAF. The black line is for BHs and the red line is for NSs.

decreasing f_{th} , as can be seen in Fig. (6). In the panel (4) of Fig. (5), we plot Ω/Ω_K as a function of radius for NSs for different f_{th} with $\dot{m} = 5 \times 10^{-3}$. It can be seen that Ω/Ω_K systematically decreases with decreasing f_{th} , which can be understood as, with a decrease of f_{th} , the radiative efficiency of the accretion flow decreases, resulting in a decrease of the angular velocity, as discussed in Section 3.1. We

list the radiative features of the ADAF around NSs for different f_{th} with $\dot{m} = 5 \times 10^{-3}$ in Table (3). We show that L_*/L_G slightly changes with changing f_{th} . It can be seen that the temperature of the thermal soft X-ray component decreases from 0.45 keV to 0.14 keV for f_{th} decreasing from 1.0 to 0.01. Meanwhile, the X-ray luminosity between 0.5 to 10 keV decreases from 1.0×10^{36} erg s^{-1} to $9.1 \times$

Table 1. Radiative features of the ADAF around BHs and NSs. T_* is the effective temperature at the surface of NSs. $L_{0.5-10\text{keV}}$ is the luminosity between 0.5 and 10 keV.

| m | R_* | α | β | f_{th} | \dot{m} | T_* (keV) | $L_{0.5-10\text{keV}}$ (erg s $^{-1}$) |
|----------|-----------|----------|---------|-----------------|--------------------|-------------|---|
| 10 (BH) | $3R_S$ | 0.3 | 0.95 | 1.0 | 5×10^{-3} | - | 2.2×10^{34} |
| 1.4 (NS) | 12.5 (km) | 0.3 | 0.95 | 1.0 | 5×10^{-3} | 0.45 | 1.0×10^{36} |

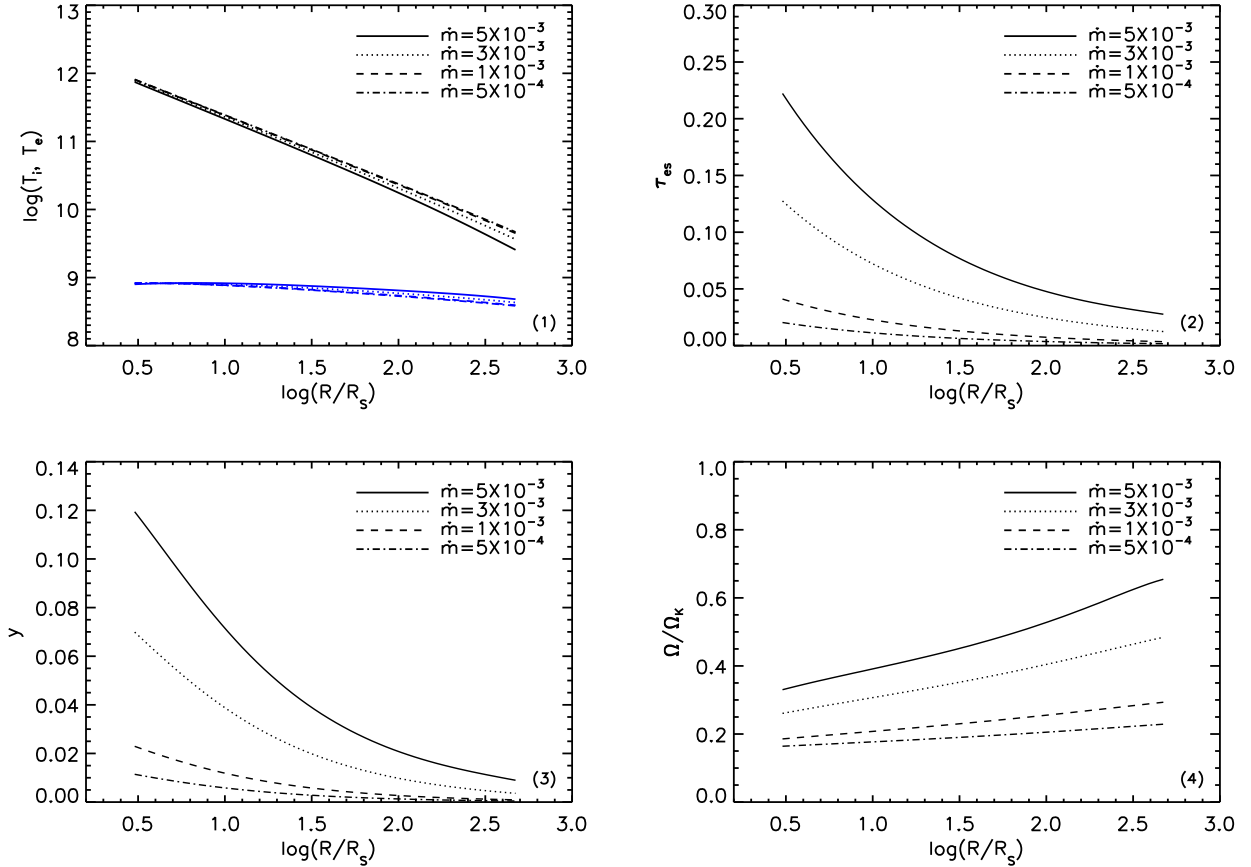

Figure 3. Panel (1): ion temperature T_i (black line) as a function of radius and electron temperature T_e (blue line) as a function of radius around NSs for different \dot{m} with $f_{\text{th}} = 1$. Panel (2): Compton scattering optical depth τ_{es} as a function of radius around NSs for different \dot{m} with $f_{\text{th}} = 1$. Panel (3): Compton y -parameter as a function of radius around NSs for different \dot{m} with $f_{\text{th}} = 1$. Panel (4): Ω/Ω_K as a function of radius around NSs for different \dot{m} with $f_{\text{th}} = 1$.

Table 2. Radiative features of the ADAF around NSs for different \dot{m} . L_*/L_G is the ratio of the energy of the ADAF transferred onto the surface of the NS per second to the accretion luminosity. T_* is the effective temperature at the surface of NSs. $L_{0.5-10\text{keV}}$ is the luminosity between 0.5 and 10 keV.

| m | R_* (km) | α | β | f_{th} | \dot{m} | L_*/L_G | T_* (keV) | $L_{0.5-10\text{keV}}$ (erg s $^{-1}$) |
|-----|------------|----------|---------|-----------------|--------------------|-----------|-------------|---|
| 1.4 | 12.5 | 0.3 | 0.95 | 1.0 | 5×10^{-3} | 56.0% | 0.45 | 1.0×10^{36} |
| 1.4 | 12.5 | 0.3 | 0.95 | 1.0 | 3×10^{-3} | 58.6% | 0.40 | 7.5×10^{35} |
| 1.4 | 12.5 | 0.3 | 0.95 | 1.0 | 1×10^{-3} | 60.8% | 0.31 | 2.7×10^{35} |
| 1.4 | 12.5 | 0.3 | 0.95 | 1.0 | 5×10^{-4} | 61.3% | 0.26 | 1.3×10^{35} |

10^{33} erg s $^{-1}$. For $f_{\text{th}} = 0.0$, there is no such a thermal soft X-ray component, and the emergent spectrum is very similar to the case of BHs with the difference only from the mass between NSs and BHs.

4 DISCUSSIONS

4.1 On the interaction between the accretion flow and the NS

In this paper, we just consider the radiative coupling between the ADAF and the NS. Specifically, we consider that the internal energy stored in the ADAF and radial kinetic energy of the

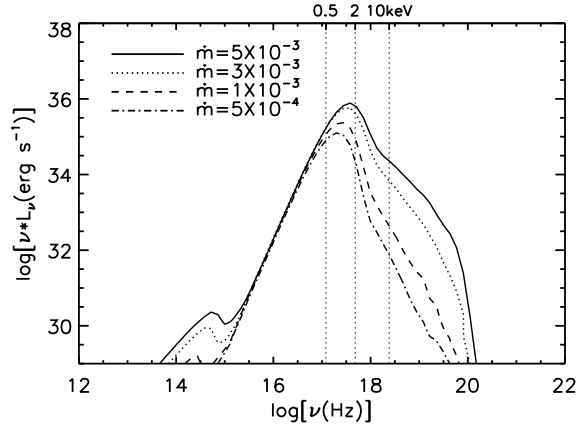


Figure 4. Emergent spectra of the ADAF around NSs for different \dot{m} with $f_{\text{th}} = 1$.

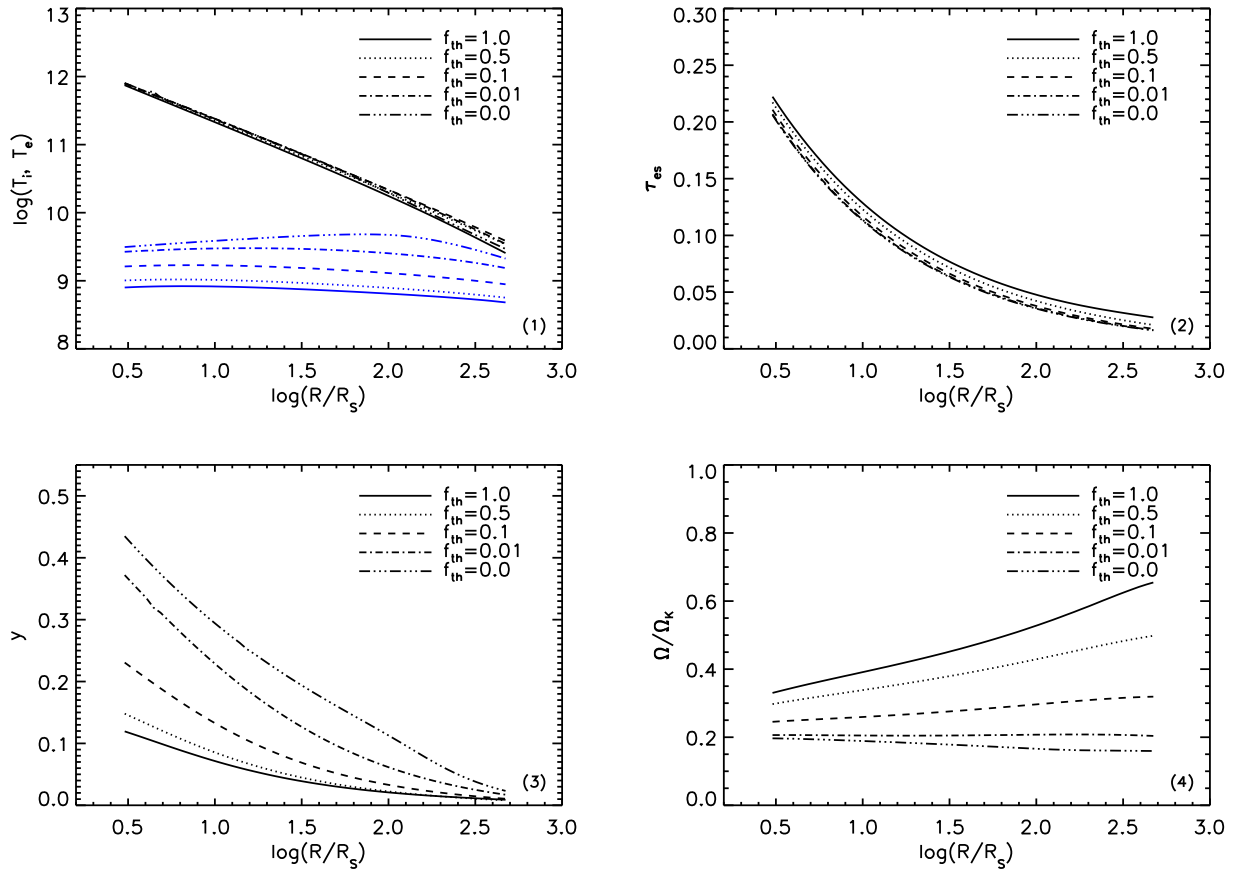


Figure 5. Panel (1): ion temperature T_i (black line) and electron temperature T_e (blue line) as a function of radius around NSs for different f_{th} with $\dot{m} = 5 \times 10^{-3}$. Panel (2): Compton scattering optical depth τ_{es} as a function of radius around NSs for different f_{th} with $\dot{m} = 5 \times 10^{-3}$. Panel (3): Compton y -parameter as a function of radius around NSs for different f_{th} with $\dot{m} = 5 \times 10^{-3}$. Panel (4): Ω/Ω_k as a function of radius around NSs for different f_{th} with $\dot{m} = 5 \times 10^{-3}$.

ADAF are transferred onto the surface of the NS. Furthermore, we assume that only a fraction, f_{th} , of this energy is thermalized at the surface of the NS as the soft photons to be scattered in the ADAF to self-consistently calculate the structure of the ADAF. The interaction between the accretion flow and the NS is complicated, one of which is the boundary layer problem

(Gilfanov & Sunyaev 2014, for review). As we have mentioned in the introduction part, there exists a critical mass accretion rate \dot{M}_{crit} . For $\dot{M} \gtrsim \dot{M}_{\text{crit}}$, the accretion flow will be in the form of a cool, geometrically thin, optically thick disc. In this case, the key point for understanding the boundary layer problem is how the accreted matter in the disc is decelerated from its Keplerian

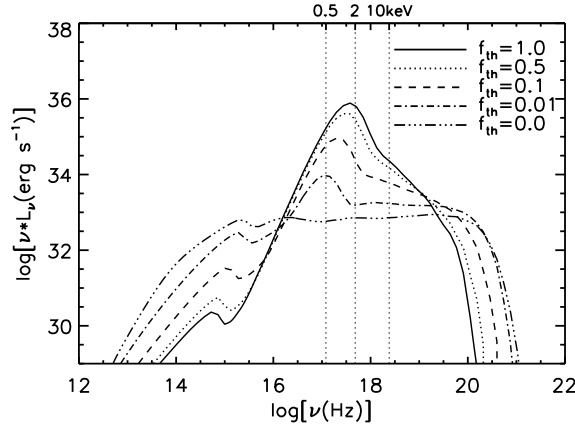


Figure 6. Emergent spectra of the ADAF around NSs for different f_{th} with $\dot{m} = 5 \times 10^{-3}$.

Table 3. Radiative features of the ADAF around NSs for different f_{th} . L_*/L_G is the ratio of the energy of the ADAF transferred onto the surface of the NS per second to the accretion luminosity. T_* is the effective temperature at the surface of NSs. $L_{0.5-10\text{keV}}$ is the luminosity between 0.5 and 10 keV.

| m | R_* (km) | α | β | f_{th} | \dot{m} | L_*/L_G | T_* (keV) | $L_{0.5-10\text{keV}}$ (erg s $^{-1}$) |
|-----|------------|----------|---------|-----------------|--------------------|-----------|-------------|---|
| 1.4 | 12.5 | 0.3 | 0.95 | 1.0 | 5×10^{-3} | 56.0% | 0.45 | 1.0×10^{36} |
| 1.4 | 12.5 | 0.3 | 0.95 | 0.5 | 5×10^{-3} | 57.3% | 0.38 | 5.5×10^{35} |
| 1.4 | 12.5 | 0.3 | 0.95 | 0.1 | 5×10^{-3} | 59.1% | 0.26 | 1.1×10^{35} |
| 1.4 | 12.5 | 0.3 | 0.95 | 0.01 | 5×10^{-3} | 60.3% | 0.14 | 9.1×10^{33} |
| 1.4 | 12.5 | 0.3 | 0.95 | 0.0 | 5×10^{-3} | 60.5% | - | 2.0×10^{33} |

orbital velocity about half the speed of light to the NS's rotational velocity, in which \sim half of the gravitational energy will be released (Popham & Narayan 1992; Narayan & Popham 1993; Inogamov & Sunyaev 1999; Popham & Sunyaev 2001). However, we think that such a boundary layer problem is not serious for the accretion with $\dot{M} \lesssim \dot{M}_{\text{crit}}$. As we know, generally, if $\dot{M} \lesssim \dot{M}_{\text{crit}}$, the accretion flow will transit from the cool, optically thick disc to the hot, optically thin ADAF. Since ADAF is hot and optically thin, intrinsically the angular velocity of the ADAF is sub-Keplerian. Because the angular velocity of the ADAF is relatively lower, as we can imagine, it is relatively easier to establish the equilibrium between ADAF and the NS. Meanwhile, because the angular velocity of the ADAF is relatively lower, the angular kinetic energy is not important compared with the internal energy and the radial kinetic energy of the ADAF. In this paper, we simply ignore the contribution of the angular kinetic energy transferred onto the surface of the NS as the soft luminosity to calculate the structure of the ADAF.

As has been shown in the panel (1), (2), (3) and (4) of Fig. 5, a change of f_{th} can significantly change the structure of the ADAF. However, we do not know the detailed physics about the interaction between the energy transferred onto the surface of the NS and the matter at the surface of the NS. Specifically, as an example, it is unclear how much of this energy can be thermalized as the soft photons for the Comptonization in the ADAF. Meanwhile, it is unclear how much of this energy is converted to other forms of energy, such as the rotational energy of the NS. As can be seen in Fig. 6, a change of f_{th} can significantly change the emergent spectra of the ADAF. We also should keep in mind that, in the present paper we do not consider the effect of the remaining fraction, $1-f_{\text{th}}$, of the energy transferred onto the surface of the NS on the emergent spectrum of the ADAF. As we mentioned, it is possible that such a

fraction of the energy could be converted to the rotational energy of the NS.

Burke et al. (2018) found that there is a clear trend between the key Comptonization properties and the NS spin for a given accretion rate in the range of $L_X/L_{\text{Edd}} \sim 0.005 - 0.1$. In the case of Newtonian approximation, the energy released in the boundary layer between the accretion flow and the NS for the Comptonization can be expressed as,

$$L_{\text{bl}} = 2\pi^2 \dot{M} R_*^2 (\nu_* - \nu_{\text{NS}})^2, \quad (14)$$

where ν_* is the rotational frequency of the accretion flow at R_* , and ν_{NS} is the rotational frequency of the NS. Here we would like to address that L_* calculated from equation (9) always dominates L_{bl} calculated from equation (14) in the framework of the ADAF solution with $\dot{m} \lesssim 5 \times 10^{-3}$ for a wide range of ν_{NS} . For example, L_* is 8.1×10^{35} erg s $^{-1}$ for $\dot{m} = 5 \times 10^{-3}$. While L_{bl} is 7.7×10^{34} erg s $^{-1}$ for $\dot{m} = 5 \times 10^{-3}$ with $\nu_{\text{NS}} = 0$, which is roughly one order of magnitude lower than that of L_* . Assuming $\nu_{\text{NS}} = 500$, L_{bl} is 2.4×10^{31} erg s $^{-1}$, which is more than four orders of magnitude lower than that of L_* . So it can be seen that the effect of NS spin on the spectrum is always not important in the ADAF case. However, we also need to note that, in the present paper, we indeed do not know how the NS spin can affect of the emergent spectrum of the ADAF if the full general relativity is considered, which will be studied in the not far future. Finally, we suggested that the value of f_{th} could be constrained by fitting the available X-ray data with high precisions, such as the X-ray data of *XMM-Newton* in the range of 0.5-10 keV, which will be done in the future work for details.

4.2 On the effect of large-scale magnetic field

As we can see, in this paper, we do not consider the effect of the strong large-scale magnetic field on the ADAF solution, which makes our solutions can only be applied to the NSs with a relatively weak magnetic field. Theoretically, if a strong large-scale magnetic field (typically $\gtrsim 10^{8-9}$ G) is existed around NSs, the geometry and the structure of the accretion flow can be changed. In this case, generally, there exists a critical radius R_M , at which the magnetic pressure is equal to the ram and gas pressure of the matter in the accretion flow. At the region of $R > R_M$, the matter of the accretion flow can roughly keep the symmetric structure in the angular direction. While at the region of $R < R_M$, the matter in the accretion flow will be gradually controlled by the magnetic field, the symmetric structure will be disrupted, forming an accretion column (Frank et al. 2002). The column accretion has very clear observational effects, i.e., the X-ray pulsar. We should note that, although it is generally believed that the strong magnetic field can significantly alter the X-ray spectrum, the observational evidence for the effect of the magnetic field on the X-ray spectrum is still in debate. Wijnands et al. (2015) compared three accreting millisecond X-ray pulsars (AMXP), i.e., IGR J18245, NGC 6440 X-2, and IGR J00291+5934 with a sample composed of 11 low-level accreting non-pulsating NSs, they did not find significant differences of the X-ray spectra in the range of 0.5-10 keV between the AMXP and the non-pulsating NSs. However, since the sample of AMXP in Wijnands et al. (2015) is very small, the authors also addressed that they can not draw any strong conclusions, i.e., a dynamically important magnetic field can change the X-ray spectra of accreting NSXRBs significantly or not.

4.3 On the effect of outflow

In this paper, a constant mass accretion rate along the radial direction is assumed to calculate the structure of the ADAF around NSs. In the history, the ADAF solution with a constant mass accretion rate was indeed applied to fit the broad-band SED of BH soft X-ray transient in quiescence (e.g. Narayan et al. 1996). However, as the analysis in (Narayan & Yi 1994), ADAF solution has a positive Bernoulli parameter (the hot nature of the ADAF), which implies that the gas is not bound to the BH. So it is suggested that ADAF solution is associated with strong outflows driven by the thermal pressure (e.g. Meier 2001; Blandford & Begelman 1999). Further, by fitting the broad-band SED of SgrA* from radio to X-rays with the ADAF, it was found that the mass accretion rate decreases with decreasing radius with a formula of $\dot{m}(r) \propto r^{0.3}$ (Yuan et al. 2003), which was confirmed by the recent hydrodynamical and magnetohydrodynamical simulations around BHs (Yuan et al. 2012a,b). Since the ADAF solution around NSs is also hot, as has been shown in this paper, we can imagine that the ADAF solution around NSs should be also associated with outflows, resulting in a decrease of the mass accretion rate with decreasing radius. If the mass accretion rate decreases with decreasing radius, both the structure and the emergent spectrum of the ADAF will change compared with a constant mass accretion rate, which of course will change the temperature of the thermal soft X-ray component as we focus in this paper. The dependence of the mass accretion rate \dot{m} on the radius r around NSs is unclear. The radius-related mass accretion rate, such as the form of $\dot{m}(r) \propto r^b$, will be considered in the future work of the detailed spectral fitting for the value of b around NSs.

5 CONCLUSIONS

In this paper, we investigate the origin of a thermal soft X-ray component detected in low-level accreting NSs based on the self-similar solution of the ADAF. We compare both the electron temperature T_e and the Compton y -parameter derived from the ADAF solution for BHs and NSs. It is found that both T_e and y of the ADAF around NSs are systematically lower than that of BHs, which consequently predicts a softer hard X-ray spectrum for NSs compared with the case for BHs. We find that the temperature of the thermal soft X-ray component decreases with decreasing mass accretion rate, which is qualitatively consistent with observations. We test the effect of f_{th} on the structure and the emergent spectrum the ADAF, with a focus on the relationship between the temperature of the thermal soft X-ray component and f_{th} . Specifically, the temperature of the thermal soft X-ray component decreases with decreasing f_{th} . We address that in the current paper, we do not consider the effect of the strong large-scale magnetic field on the ADAF, which makes that our solution can only be applied to NSs with a relatively weak magnetic field. We discuss the importance of the outflows on the emergent spectrum of the ADAF around NSs. Finally, We suggest that the detailed X-ray spectral fitting can help to constrain the model parameters, such as f_{th} , in the future work.

ACKNOWLEDGMENTS

We thank the anonymous referee for his/her very expert comments and suggestions. This work is supported by the National Natural Science Foundation of China (Grants 11773037 and 11673026), the gravitational wave pilot B (Grants No. XDB23040100), and the National Program on Key Research and Development Project (Grant No. 2016YFA0400804).

REFERENCES

- Abramowicz M. A., Chen X., Kato S., Lasota J.-P., Regev O., 1995, *ApJ*, **438**, L37
- Armas Padilla M., Degenaar N., Wijnands R., 2013a, *MNRAS*, **434**, L586
- Armas Padilla M., Wijnands R., Degenaar N., 2013b, *MNRAS*, **436**, L89
- Armas Padilla M., Wijnands R., Degenaar N., 2013c, *MNRAS*, **436**, L89
- Bahramian A., et al., 2014, *ApJ*, **780**, 127
- Blandford R. D., Begelman M. C., 1999, *MNRAS*, **303**, L1
- Burke M. J., Gilfanov M., Sunyaev R., 2017, *MNRAS*, **466**, 194
- Burke M. J., Gilfanov M., Sunyaev R., 2018, *MNRAS*, **474**, 760
- Campana S., Brivio F., Degenaar N., Mereghetti S., Wijnands R., D'Avanzo P., Israel G. L., Stella L., 2014, *MNRAS*, **441**, 1984
- Chen X., Abramowicz M. A., Lasota J.-P., Narayan R., Yi I., 1995, *ApJ*, **443**, L61
- Degenaar N., Wijnands R., Miller J. M., 2013a, *ApJ*, **767**, L31
- Degenaar N., Miller J. M., Wijnands R., Altamirano D., Fabian A. C., 2013b, *ApJ*, **767**, L37
- Done C., Gierliński M., Kubota A., 2007, *A&ARv*, **15**, 1
- Frank J., King A., Raine D. J., 2002, *Accretion Power in Astrophysics: Third Edition*
- Garcia M. R., McClintock J. E., Narayan R., Callanan P., Barret D., Murray S. S., 2001, *ApJ*, **553**, L47
- Gilfanov M., 2010, in Belloni T., ed., *Lecture Notes in Physics*, Berlin Springer Verlag Vol. 794, *Lecture Notes in Physics*, Berlin Springer Verlag. p. 17 ([arXiv:0909.2567](https://arxiv.org/abs/0909.2567)), doi:10.1007/978-3-540-76937-8_2
- Gilfanov M. R., Sunyaev R. A., 2014, *Physics Uspekhi*, **57**, 377
- Gladstone J., Done C., Gierliński M., 2007, *MNRAS*, **378**, 13
- Hameury J.-M., Barret D., Lasota J.-P., McClintock J. E., Menou K., Motch C., Olive J.-F., Webb N., 2003, *A&A*, **399**, 631

- Hernandez Santisteban J. V., et al., 2018, preprint, ([arXiv:1801.03006](https://arxiv.org/abs/1801.03006))
- Ichimaru S., 1977, *ApJ*, **214**, 840
- Inogamov N. A., Sunyaev R. A., 1999, *Astronomy Letters*, **25**, 269
- Jonker P. G., Galloway D. K., McClintock J. E., Buxton M., Garcia M., Murray S., 2004, *MNRAS*, **354**, 666
- Kubota A., Done C., 2004, *MNRAS*, **353**, 980
- Lasota J.-P., 2000, *A&A*, **360**, 575
- Maccarone T. J., 2003, *A&A*, **409**, 697
- Maccarone T. J., Coppi P. S., 2003, *MNRAS*, **338**, 189
- Mahadevan R., 1997, *ApJ*, **477**, 585
- Manmoto T., Mineshige S., Kusunose M., 1997, *ApJ*, **489**, 791
- McClintock J. E., Narayan R., Rybicki G. B., 2004, *ApJ*, **615**, 402
- Meier D. L., 2001, *ApJ*, **548**, L9
- Menou K., Esin A. A., Narayan R., Garcia M. R., Lasota J.-P., McClintock J. E., 1999, *ApJ*, **520**, 276
- Merloni A., Heinz S., di Matteo T., 2003, *MNRAS*, **345**, 1057
- Meyer-Hofmeister E., Liu B. F., Meyer F., 2005, *A&A*, **432**, 181
- Narayan R., McClintock J. E., 2008, *New Astron. Rev.*, **51**, 733
- Narayan R., Popham R., 1993, *Nature*, **362**, 820
- Narayan R., Yi I., 1994, *ApJ*, **428**, L13
- Narayan R., Yi I., 1995, *ApJ*, **452**, 710
- Narayan R., McClintock J. E., Yi I., 1996, *ApJ*, **457**, 821
- Nowak M. A., Wilms J., Dove J. B., 2002, *MNRAS*, **332**, 856
- Popham R., Narayan R., 1992, *ApJ*, **394**, 255
- Popham R., Sunyaev R., 2001, *ApJ*, **547**, 355
- Qiao E., Liu B. F., 2010, *PASJ*, **62**, 661
- Qiao E., Liu B. F., 2013, *ApJ*, **764**, 2
- Rees M. J., Begelman M. C., Blandford R. D., Phinney E. S., 1982, *Nature*, **295**, 17
- Remillard R. A., McClintock J. E., 2006, *ARA&A*, **44**, 49
- Rodriguez J., Corbel S., Tomsick J. A., 2003, *ApJ*, **595**, 1032
- Shakura N. I., Sunyaev R. A., 1973, *A&A*, **24**, 337
- Stepney S., 1983, *MNRAS*, **202**, 467
- Sunyaev R. A., Titarchuk L., 1989, in Hunt J., Battrick B., eds, *ESA Special Publication Vol. 296, Two Topics in X-Ray Astronomy, Volume 1: X-Ray Binaries. Volume 2: AGN and the X-Ray Background.*
- Sunyaev R. A., et al., 1991, *Broadband X-Ray Spectra of Black-Hole Candidates X-Ray Pulsars and Low-Mass Binary X-Ray Systems - KVANT Module Results*
- Tanaka Y., Lewin W. H. G., 1995, *X-ray Binaries*, pp 126–174
- Wijnands R., Degenaar N., Armas Padilla M., Altamirano D., Cavecchi Y., Linares M., Bahramian A., Heinke C. O., 2015, *MNRAS*, **454**, 1371
- Xie F.-G., Yuan F., 2012, *MNRAS*, **427**, 1580
- Yuan F., Narayan R., 2014, *ARA&A*, **52**, 529
- Yuan F., Quataert E., Narayan R., 2003, *ApJ*, **598**, 301
- Yuan F., Wu M., Bu D., 2012a, *ApJ*, **761**, 129
- Yuan F., Bu D., Wu M., 2012b, *ApJ*, **761**, 130
- Zampieri L., Turolla R., Zane S., Treves A., 1995, *ApJ*, **439**, 849
- Zhang H., Yu W.-F., 2018, *Research in Astronomy and Astrophysics*, **18**, 033
- Zhang Z., Sakurai S., Makishima K., Nakazawa K., Ono K., Yamada S., Xu H., 2016, *ApJ*, **823**, 131
- van den Eijnden J., et al., 2018, *MNRAS*, **475**, 2027

This paper has been typeset from a $\text{\TeX}/\text{\LaTeX}$ file prepared by the author.